

Self-similar dynamics of order parameter fluctuations in pump-probe experiments

Pavel E. Dolgirev,^{1,*} Marios H. Michael,¹ Alfred Zong,² Nuh Gedik,² and Eugene Demler¹

¹*Department of Physics, Harvard University, Cambridge, Massachusetts 02138, USA.*

²*Massachusetts Institute of Technology, Department of Physics, Cambridge, Massachusetts 02139, USA.*

(Dated: June 9, 2022)

Upon excitation by a laser pulse, broken-symmetry phases of a wide variety of solids demonstrate similar order parameter dynamics characterized by a dramatic slowing down of relaxation for stronger pump fluences. Motivated by this recurrent phenomenology, we develop a simple non-perturbative effective model for photoinduced dynamics of collective bosonic excitations. We find that as the system recovers after photoexcitation, it shows universal prethermalized dynamics manifesting a power-law, as opposed to exponential, relaxation, explaining the slowing down of the recovery process. For strong quenches, long-wavelength over-populated transverse modes dominate the long-time dynamics; their distribution function exhibits universal scaling in time and space, whose universal exponents can be computed analytically. Our model offers a unifying description of order parameter fluctuations in a regime far from equilibrium, and our predictions can be tested with available time-resolved techniques.

I. INTRODUCTION

In the theory of equilibrium phase transitions, the concept of universality plays a central role because it allows describing a plethora of experimentally studied thermal phase transitions with just a few universality classes¹. For systems far from equilibrium, the notion of universality is relatively unexplored and has recently emerged as an active field^{2–10}, partially motivated by recent progress in ultracold-atom^{11–14} and ultrafast pump-probe experiments¹⁵. In a non-equilibrium context, one of the dramatic manifestations of universality is the emergence of the self-similar evolution of correlation functions¹⁶. In particular, after a strong perturbation, the transient equal-time two-point correlation function $D(|\mathbf{x} - \mathbf{y}|, t)$ might depend only on a single evolving length scale $\xi(t)$ and two universal functions:

$$D(|\mathbf{x} - \mathbf{y}|, t) = g(t)f(|\mathbf{x} - \mathbf{y}|/\xi(t)). \quad (1)$$

Functional forms of $f(x)$ and $g(t)$ depend neither on microscopic parameters nor on initial conditions. Typical equations of motion, often a complex system of partial integro-differential equations, represent an interplay between many degrees of freedom such as quasiparticles, order parameter (OP), phonons and/or magnons. If these equations allow for the above self-similar form, the analysis might reduce to just a few differential equations, which is particularly appealing since it eases the interpretation of the involved evolution. From a physical standpoint, the self-similarity suggests a stabilization-like mechanism, which is usually associated with the transport of a conserved quantity.

Several recurrent observations in experiments also hint at the existence of universality in the out-of-equilibrium context. Aided by recent advances in pump-probe techniques, light-induced phase transitions have been investigated in a wide variety of materials, including charge-density-wave (CDW) compounds^{15,17–27}, putative excitonic insulators^{28,29}, magnetically-ordered systems^{30,31},

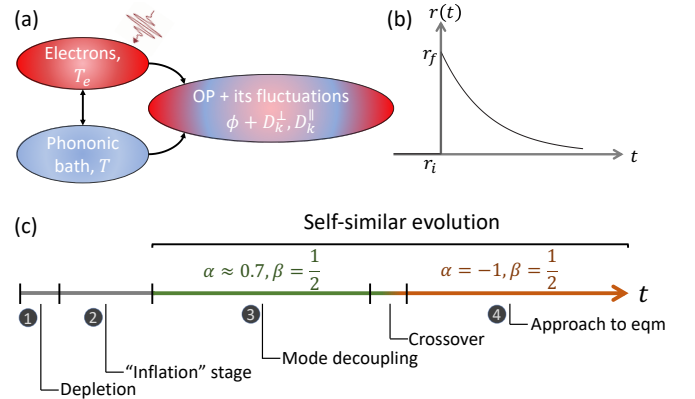


FIG. 1. (a) Schematics of a non-equilibrium state: electrons (red) and the phononic bath (blue) are thermal with temperatures $T_e(t)$ and T , respectively; the OP subsystem (mixed colors) is not assumed to be thermal. (b) Time evolution of the Landau coefficient $r(t)$ [Eq. (13)]. It mimics a photoexcitation event in (a). (c) Schematics of dynamical stages. During stages 3 and 4, the system exhibits self-similarity. Green and orange distinguish the scaling exponents, α and β [Eq. (15)], in these two stages.

and systems that exhibit several intertwined orders^{32,33}. Upon photoexcitation, some general phenomenology is observed: (i) The recovery of a photo-suppressed OP takes longer at stronger pump pulse fluence; (ii) The amplitude of the OP restores faster than the phase, exhibiting a separation of timescales; (iii) Related to (ii), peaks in diffraction experiments remain broadened compared to equilibrium shape long after photoexcitation, showing prolonged suppression of long-range phase coherence. Our subsequent analysis is generic; however, for concreteness, we focus here on LaTe_3 , an incommensurate CDW material, where all of these findings were confirmed in the same set of experiments¹⁹. These observations hence motivate us to search for a unified theoretical description.

A common approach to describing many-body dynamics in symmetry-broken states is based on the so-called

three-temperature model (3TM)^{34–38}. In this framework, a non-equilibrium state is characterized by assigning different temperatures to different subsystems, such as electrons, phonons, and OP degrees of freedom³⁹. Upon photoexcitation, most incoming light is absorbed by electrons, instantaneously increasing the electronic temperature, T_e . The introduction of $T_e(t)$ is justified provided we are only interested in phononic timescales sufficiently exceeding the fast electron-electron scattering time. Subsequent dynamics corresponds to heat exchange between hot electrons and the other two subsystems. In this process, it is often assumed that the lattice heating is negligible because the lattice heat capacity at room temperature is several orders in magnitude larger than that of electrons. Even though the 3TM suggests an intuitive picture about the interplay among different subsystems, it often lacks theoretical justification. In particular, low-energy, low-momenta Goldstone modes can be easily excited in the symmetry-broken phase. Hence, one key assumption in the 3TM that the OP subsystem remains thermal is a crude over-simplification.

In the present paper, we go beyond the 3TM and formulate a general theory of out-of-equilibrium OP correlations to account for potentially non-thermal states of the OP subsystem – see Fig. 1a. Our theory focuses on nonlinear dynamics of collective bosonic excitations. This should be contrasted to earlier work on the relaxation of quasiparticles in superconductors, in which recombination dynamics can lead to faster relaxation rates for higher quasiparticle densities^{40–42} (see, however, Ref. 43). Within our effective bosonic model, we find that upon photoexcitation, the system passes through four dynamical stages outlined in Fig. 1c. For a strong quench, not only is the OP subsystem far from being thermal but overpopulated slow Goldstone modes fully dominate the intrinsic evolution at long times. Even more strikingly, in the last two dynamical stages in Fig. 1c, the distribution function of these modes exhibits self-similar evolution as in Eq. (1). These findings provide an intuitive physical interpretation of the mentioned phenomenology, as we elucidate below.

The paper is organized as follows. In Sec. II, we develop the aforementioned model of pump-probe experiments. Within this framework, the response to an applied laser pulse and the four dynamical stages are elaborated in Sec. III. Section IV is devoted to the universality present in the last two dynamical stages. Section V contains further discussion on the applicability of the present theory to real experiments.

II. THEORETICAL FRAMEWORK

Spontaneous symmetry breaking (SSB) is described by the time-dependent Landau-Ginzburg formalism (model-A in Ref. 44):

$$\frac{d\phi_\alpha(\mathbf{x}, t)}{dt} = -\Gamma \frac{\delta \mathcal{F}}{\delta \phi_\alpha(\mathbf{x}, t)} + \eta_\alpha(\mathbf{x}, t). \quad (2)$$

Here ϕ_α is an N -component vector of real fields representing the OP. The free energy functional reads

$$\mathcal{F}[\phi] = \int d^3\mathbf{x} \left[\frac{r}{2} \phi_\alpha^2 + \frac{K}{2} (\nabla \phi_\alpha)^2 + u(\phi_\alpha^2)^2 \right], \quad (3)$$

and η_α represents the noise originating from the phononic bath at temperature T :

$$\langle \eta_\alpha(\mathbf{x}, t) \eta_\beta(\mathbf{x}', t') \rangle = 2T\Gamma \delta_{\alpha,\beta} \delta(\mathbf{x} - \mathbf{x}') \delta(t - t'). \quad (4)$$

Here r , K , u , and Γ are the model parameters. For homogeneous quenches, without loss of generality, we assume that SSB occurs along the first direction: $\phi(t) = \langle \phi_1(\mathbf{x}, t) \rangle$. Associated with the OP are longitudinal (Higgs modes) $D_{\mathbf{k}}^{\parallel}(t) \equiv \langle \phi_1(\mathbf{k}; t) \phi_1(-\mathbf{k}; t) \rangle_c$ and transverse (Goldstone modes) $D_{\mathbf{k}}^{\perp}(t) \equiv \langle \phi_{\alpha \neq 1}(\mathbf{k}; t) \phi_\alpha(-\mathbf{k}; t) \rangle_c$ correlation functions. The model-A formalism in Eqs. (2)–(4) can be conveniently rewritten in terms of the Fokker-Planck equation:

$$\partial_t \mathcal{P} = T\Gamma \sum_{\mathbf{k}, \alpha} \frac{\delta}{\delta \phi_{\alpha, \mathbf{k}}} \left[\frac{\mathcal{P}}{T} \frac{\delta \mathcal{F}}{\delta \phi_{\alpha, -\mathbf{k}}} + \frac{\delta \mathcal{P}}{\delta \phi_{\alpha, -\mathbf{k}}} \right], \quad (5)$$

where $\mathcal{P}([\phi], t)$ is the probability distribution functional of space-dependent field configurations $\phi_\alpha(\mathbf{x})$. To the leading order in $1/N$, $\mathcal{P}([\phi], t)$ is Gaussian, implying that the OP $\phi(t)$ and the correlators $D_{\mathbf{k}}^{\parallel}(t)$, $D_{\mathbf{k}}^{\perp}(t)$ form a closed set of dynamical variables. The self-consistent equations of motion read^{45,46} (see Appendix A for a derivation)

$$\frac{d\phi(t)}{dt} = -\Gamma r_{\text{eff}} \phi, \quad (6)$$

$$\frac{dD_{\mathbf{k}}^{\perp}(t)}{dt} = 2T\Gamma - 2\Gamma(K\mathbf{k}^2 + r_{\text{eff}})D_{\mathbf{k}}^{\perp}, \quad (7)$$

$$\frac{dD_{\mathbf{k}}^{\parallel}(t)}{dt} = 2T\Gamma - 2\Gamma(K\mathbf{k}^2 + r_{\text{eff}} + 8u\phi^2)D_{\mathbf{k}}^{\parallel}. \quad (8)$$

Here the self-consistent “mass”-term is defined as

$$r_{\text{eff}}(t) = r(t) + 4u \left(\phi^2 + n_{\text{tot}}^{\parallel} + (N-1)n_{\text{tot}}^{\perp} \right), \quad (9)$$

where $n_{\text{tot}}^{\perp(\parallel)} \equiv \int^{\Lambda} \frac{d^3\mathbf{q}}{(2\pi)^3} D_{\mathbf{q}}^{\perp(\parallel)}$, Λ is the UV-cutoff. Note that quantities such as energy or total number of excitations are not conserved due to the external bath.

The bath, cf. Eq. (4), will also always result in the thermalization of the system, in contrast to quenches in the isolated $O(N)$ model, where, to the leading in $1/N$ order, the system does not demonstrate equilibration^{47–51}. In that case, thermalization occurs only after subleading corrections are taken into consideration⁵². As such, the presence of the external bath in our case motivates us to disregard these subleading corrections here.

From the equations of motion, we obtain the equilibrium correlators:

$$D_{\mathbf{k}}^{\parallel} = \frac{T}{K\mathbf{k}^2 + 8u\phi^2 + r_{\text{eff}}}, \quad D_{\mathbf{k}}^{\perp} = \frac{T}{K\mathbf{k}^2 + r_{\text{eff}}}. \quad (10)$$

This result is a manifestation of the equipartition theorem. In the symmetry broken phase, where $r_{\text{eff}} = 0$ and $\phi \neq 0$, we observe that the OP equilibrium value ϕ is affected by the thermal fluctuations, cf. Eq. (9). The transverse correlation length $\xi_{\perp} \propto r_{\text{eff}}^{-1/2}$ is divergent. In the disordered phase, $r_{\text{eff}} \neq 0$ and $\phi = 0$, the transverse and longitudinal correlations are not distinguishable.

A useful point of view on the above approximations is as follows. The equations of motion (6)-(9) are equivalent to

$$\frac{d\delta\phi_{\mathbf{k}}^{\perp}(t)}{dt} = -\Gamma(K\mathbf{k}^2 + r_{\text{eff}})\phi_{\mathbf{k}}^{\perp} + \eta_{\mathbf{k}}^{\perp}(t), \quad (11)$$

$$\frac{d\delta\phi_{\mathbf{k}}^{\parallel}(t)}{dt} = -\Gamma(K\mathbf{k}^2 + r_{\text{eff}} + 8u\phi^2)\phi_{\mathbf{k}}^{\parallel} + \eta_{\mathbf{k}}^{\parallel}(t), \quad (12)$$

where $\delta\phi_{\mathbf{k}}^{\alpha}$ represents the fluctuating part of the corresponding Fourier mode $\phi_{\mathbf{k}}^{\alpha}$. We observe that each of the fluctuating modes lives in an effectively parabolic potential, $\langle\delta\phi_{\mathbf{k}}^{\alpha}\rangle = 0$, and the noise term establishes the equilibrium variances given by Eq. (10).

We now formulate the quenching protocol. For simplicity, we assume that the electronic temperature T_e cools down to the equilibrium value T with a constant rate τ_{QP} defined by the electron-phonon coupling. This assumption seems to be not too crude for LaTe_3 , where the Fermi surface is only partially gaped, and the excited by the laser pulse electrons can relax through a gapless channel^{19,37}. For a different situation, our framework should be straightforwardly extended. In the usual Landau-Ginzburg theory, the coefficient $r(T_e)$ depends linearly on T_e . To mimic a photoexcitation event, we therefore impose the following dynamics on $r(t)$ (Fig. 1b):

$$r(t) = r_i + \theta(t) \exp(-t/\tau_{\text{QP}}) \times (r_f - r_i), \quad (13)$$

where $\theta(t)$ is the Heaviside theta function, r_i is the pre-pulse value chosen such that $\phi \neq 0$, and $(r_f - r_i)$ characterizes the pulse strength. Below we focus on time delays much beyond τ_{QP} .

In the next section, we apply the above theoretical framework to investigate the intrinsic dynamics after the arrival of a laser pulse. Our conclusions are not specific to the choice of model parameters, but in the numerical simulations below, we fix them to roughly mimic the experimental results in Ref. 19. There, the values of Γ and τ_{QP} are expected to be similar.

III. EVOLUTION AFTER PHOTOEXCITATION

Upon photoexcitation, cf. Eq. (13), the system passes through four dynamical stages (Fig. 1c) – (i) depletion, (ii) inflation, (iii) mode decoupling and (iv) relaxation to the thermal equilibrium. We cover each of them below.

In Fig. 2a, we show numerical results for the dynamics of the OP, $\phi(t)$. For a weak pump, $\phi(t)$ becomes slightly suppressed and then quickly recovers to the initial value ϕ_0 . This should be contrasted to the case

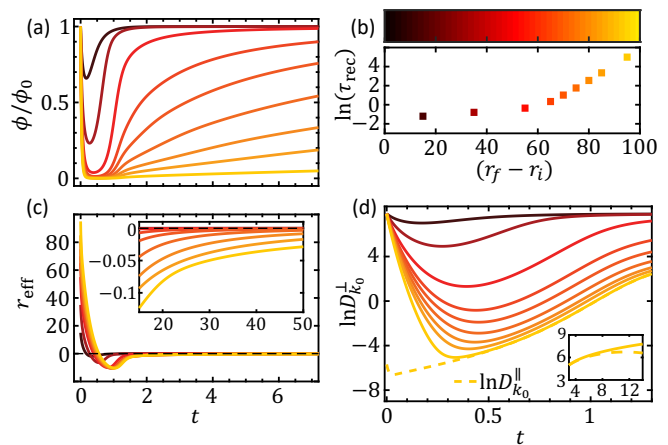


FIG. 2. Intrinsic dynamics for different quench strengths, $(r_f - r_i)$. (a) Time dependence of the OP, $\phi(t)$, normalized by its pre-pulse value ϕ_0 . At long times, $(\phi(t) - \phi_0) \sim t^{-d_\phi}$ with $d_\phi = \frac{3}{2}$. (b) OP recovery time τ_{rec} . (c) Dynamics of $r_{\text{eff}}(t)$. Initially, large positive r_{eff} is suppressed and becomes negative; then it slowly restores as $r_{\text{eff}} \sim t^{-d_r}$ with $d_r = \frac{5}{2}$ to zero. Inset: Zoomed-in view on the long-time tails. (d) Evolution of $D_{k_0}^{\perp}$, where $k_0 = \frac{2\pi}{L}$ is the lowest wave vector used in our calculations ($L = 1000$). For a strong pulse, initially $D_{k_0}^{\perp}$ is suppressed to almost zero; after r_{eff} changes sign, it exponentially proliferates. Dotted line corresponds to $D_{k_0}^{\parallel}$ for the strongest pulse considered. $D_{k_0}^{\parallel}$ and $D_{k_0}^{\perp}$ very soon merge into a single curve, indicating that the OP is melted. Inset: longer time dynamics for the strongest pulse; $D_{k_0}^{\parallel}$ and $D_{k_0}^{\perp}$ become distinguishable once the OP value $\phi(t)$ becomes appreciable. Throughout the paper, we use the following parameters: $K = u = 1$, $N = 4$, $\Lambda = \pi$, $\Gamma = 0.5$, $\tau_{\text{QP}} = 0.3$, $r_i = -15$, $T = 0.1$. All panels share the same color scale in (b) for the quench strengths.

of a strong pulse, for which initially the OP becomes strongly suppressed and then goes through a long recovery process. The recovery takes longer for stronger pulses (Fig. 2b). This slowing-down is due to the power-law dynamics $\delta\phi(t) \equiv (\phi(t) - \phi_0) \sim t^{-d_\phi}$ with $d_\phi = \frac{3}{2}$, which we further discuss in the next section.

In Fig. 2c, we plot the evolution of $r_{\text{eff}}(t)$. Upon arrival of a laser pulse, $r_{\text{eff}}(+0) = (r_f - r_i)$. This large initial value first decreases due to the time evolution of the “bare value” of $r(t)$, cf. Eq. (13), and later, at $t \gtrsim \tau_{\text{QP}}$, due to the dynamics of the OP and collective modes described by Eqs. (6)–(8). Even though $r(t)$ returns to its equilibrium value r_i during a relatively short time τ_{QP} , dynamics of r_{eff} occurs over much longer time scale where it even changes sign (Fig. 2c). We find that long-time evolution of $r_{\text{eff}} \sim t^{-d_r}$ is power-law-like with $d_r = \frac{5}{2}$. For the fluctuating modes $\delta\phi_{\mathbf{k}}^{\alpha}$, a large value of r_{eff} implies that each of the effective parabolic potentials becomes initially steeper, and, as such, the noise term in Eq. (4) tends to depopulate these modes (Fig. 2d). Therefore, the first stage – *depletion* – is characterized by suppression of the OP and correlations $D_{\mathbf{k}}^{\perp}$ and $D_{\mathbf{k}}^{\parallel}$.

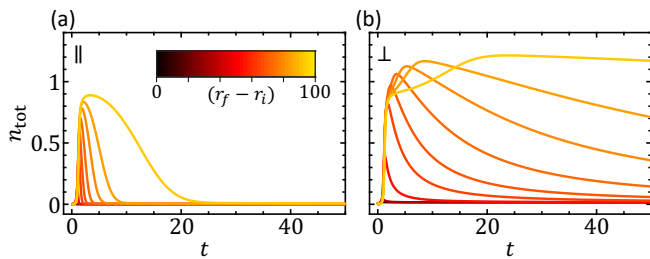


FIG. 3. Separation of timescales. (a) Long-time dynamics of the total population of longitudinal modes, $n_{\text{tot}}^{\parallel}(t)$. (b) The same for transverse modes, $n_{\text{tot}}^{\perp}(t)$. When $n_{\text{tot}}^{\parallel}$ is nearly fully recovered, n_{tot}^{\perp} approaches its maximum.

The second stage – *inflation* – starts when r_{eff} changes its sign. A negative r_{eff} implies that each of the effective parabolic potentials becomes shallower or, as the case for the low-momenta transverse modes, can even become inverted. Therefore, during the inflation, population in each of the modes proliferates, most dramatically for the low-momenta modes (Fig. 2d).

For a strong quench and at the time when the OP becomes completely suppressed, the longitudinal and transverse correlations are no longer distinguishable (Fig. 2d). This parallels the disordered phase in equilibrium situation. As the OP develops, these modes start to separate. We will associate the end of the inflation stage with the time when $D_{\mathbf{k}=0}^{\parallel}$ reaches its maximum value (see inset in Fig. 2d, dashed curve).

Because of the additional correction to the quadratic term for the longitudinal correlations in Eq. (8), the subsequent evolution – *mode decoupling* – is very different for the longitudinal and transverse modes; see Fig. 3. The longitudinal correlations start to relax back to the thermal equilibrium value in Eq. (10), while the transverse modes continue to proliferate, resulting in the exponent α , cf. Eq. (15), being positive during the third dynamical stage. Moreover, by the time when $n_{\text{tot}}^{\parallel}$ is sufficiently recovered, n_{tot}^{\perp} is about to reach its maximum. Strong experimental evidence of this separation of timescales was reported in Refs. 19, 24, and 25.

Just after the mode decoupling, n_{tot}^{\perp} starts to slowly decrease, cf. Eq. (16), suggesting that the system enters the final relaxation stage. Note that even though lowest-momenta modes $D_{\mathbf{k}}^{\perp}$ continue to proliferate at very long times, their relative contribution to n_{tot}^{\perp} is suppressed by the reduced phase space of these modes, which is proportional to k^2 . The underlying dynamics is reminiscent of an inverse particle cascade in the theory of turbulence^{8,53,54}. The main difference is that in our system the dynamics is overdamped.

In the next section, we focus on the last two dynamical stages, where we find that the system exhibits self-similar scalings in time and space, manifesting power-law-like, as opposed to exponential, behavior.

IV. UNIVERSALITY IN THE INTRINSIC DYNAMICS

Our discovery of self-similarity can be summarized in the following equations. The distribution function of the Goldstone modes follows

$$\delta D_{\mathbf{k}}^{\perp}(t) \simeq \frac{g(t)}{k^2} f(k/k_{\perp}^*(t)), \quad (14)$$

where $\delta D_{\mathbf{k}}^{\perp}(t) \equiv (D_{\mathbf{k}}^{\perp}(t) - D_{\mathbf{k},eq}^{\perp})$ and $D_{\mathbf{k},eq}^{\perp}$ is the pre-pulse equilibrium distribution given by Eq. (10). The form in Eq. (14) is similar to the one in Eq. (1), though written in momentum space; $\xi_{\perp}(t) \equiv (k_{\perp}^*(t))^{-1}$ represents the emergent time-dependent length scale. We also identify the scaling relations

$$g(t) \sim t^{\alpha}, k_{\perp}^* \sim t^{-\beta}. \quad (15)$$

Both power-law exponents α , β and the function $f(x)$ are universal. We find that $\beta = \frac{1}{2}$; $\alpha \approx 0.7$ at early times while $\alpha = -1$ in the final relaxation stage. The scaling functions $f(x)$, $k_{\perp}^*(t)$, and $g(t)$ are shown in Fig. 4. In a model where one retains dissipation but neglects the noise coming from the bath, an exponential behavior is expected instead⁵⁵.

We first explore the implications of the self-similarity in Eq. (14) on the experimental phenomenology. Prior to the arrival of the pump pulse, the system possesses long-range coherence manifested in the macroscopic homogeneous OP ϕ and divergent transverse correlation length $\xi_{\perp} = \infty$. The laser pulse depletes this coherence. Eq. (14) suggests that as the system evolves towards equilibrium, it develops a finite correlation length $\xi_{\perp}(t)$ that slowly grows in a diffusive manner⁵⁶ $\xi_{\perp}(t) \sim \sqrt{t}$, consistent with recent experiments^{24,25}. This physical picture explains the broadening of diffraction peaks observed long after the arrival of the pulse. The slowing-down of the OP recovery can also be deduced from Eq. (14). The system enters the final dynamical stage with $g(t) \simeq A_Q t^{-1}$, where A_Q is a constant of proportionality that monotonically increases with the quench strength. By contrast, as shown in Fig. 4c, $k_{\perp}^*(t)$ does not depend on the quench. Therefore, the cumulative effect, expressed in the change of the population of transverse modes $\delta n_{\text{tot}}^{\perp}$, behaves as

$$\delta n_{\text{tot}}^{\perp} \equiv \int \frac{d^3\mathbf{k}}{(2\pi)^3} \delta D_{\mathbf{k}}^{\perp}(t) \sim A_Q t^{-3/2}, \quad (16)$$

i.e. as a *power-law*. Since the transverse modes dominate the long-time dynamics, from Eq. (16) it follows that characteristic recovery time $\tau_{\text{rec}} \sim A_Q^{2/3}$ is a monotonically increasing function of the quench strength (Fig. 2b).

In the following, we offer a formal derivation of all the long-time power-law exponents: $\beta = \frac{1}{2}$, $\alpha = -1$, $d_{\phi} = \frac{3}{2}$, and $d_r = \frac{5}{2}$. Re-establishing the long-range coherence, which is depleted by the laser pulse, is the *slowest* process that happens in the system, $k_{\perp}^* \sim t^{-\beta}$. Motivated by the numerical results in Figs. 2 and 4, let us assume that

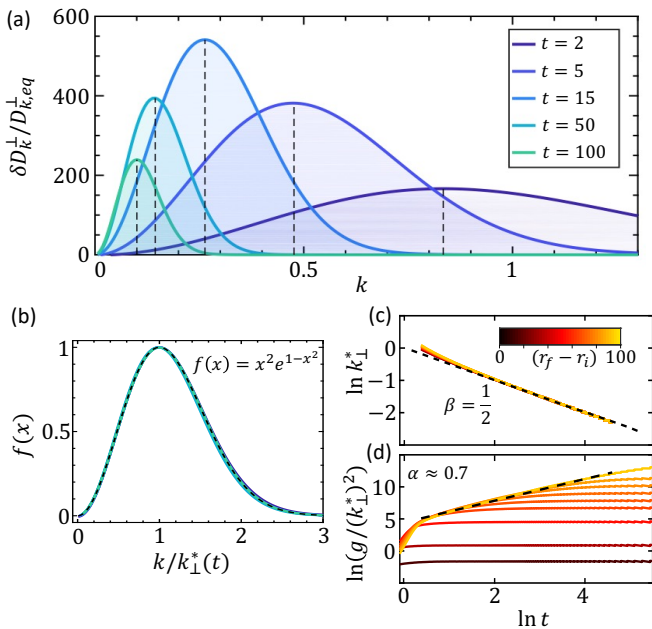


FIG. 4. Long-time self-similarity. (a) Time dependence of the change in transverse momentum distribution δD_k^\perp normalized by the equilibrium value in Eq. (10). Quench strength is set to be $(r_f - r_i) = 80$. Dashed lines track the position of the peak, $k_\perp^*(t)$; $g(t)$ corresponds to the peak height. (b) Rescaled curves collapse into $f(x)$ [Eq. (14)]. (c) Evolution of $k_\perp^*(t) \sim t^{-\frac{1}{2}}$ at different quench strengths. Note that $k_\perp^*(t)$ does not depend on quench. (d) The same for the scaling function $g(t)$. From this figure we extract $\alpha \approx 0.7$ in the third dynamical stage and $\alpha = -1$ in the final stage [Eq. (15)].

$d_r > 2\beta$, which will turn out to be consistent with the subsequent derivation. We note that the most relevant transverse modes are the ones with wave vectors close to k_\perp^* , cf. Fig. 4. For these modes, we can safely neglect fast $r_{\text{eff}} \sim t^{-d_r}$ in Eq. (7) compared to slow $(k_\perp^*)^2 \sim t^{-2\beta}$, resulting in a simple diffusion-like equation with the solution $\delta D_k^\perp = A_k \exp(-2\Gamma k^2 t)$, where A_k is yet an unknown function of k . As supported by Fig. 2d, $\delta D_k^\perp(t)$ does not diverge for $k \rightarrow 0$. One may then Taylor-expand A_k as $A_k = A_0 + A_2 k^2 + A_4 k^4 + \dots$. The relevant k vectors, the ones in the vicinity of $k_\perp^*(t)$, are small at long times, and, thus, it is safe to leave only the dominant harmonic A_0 in this expansion, i.e. $\delta D_k^\perp \sim \exp(-2\Gamma k^2 t)$, consistent with $\beta = \frac{1}{2}$ and $\alpha = -1$, cf. also Fig. 4b.

To extract the value of d_r , we need to consider the interplay between the OP and transverse correlations (longitudinal correlations are discussed in Appendix B). Assuming that at long times $r_{\text{eff}} \sim t^{-d_r}$, the equation of motion (6) reads $\frac{d}{dt} \delta \phi = -\Gamma r_{\text{eff}}(t) \phi \sim t^{-d_r}$, where we implied that $\phi(t) = \phi_0 + \delta \phi(t)$ is already close to its equilibrium value ϕ_0 . By integrating the above equation, we obtain $\phi^2(t) \approx \phi_0^2 + C t^{-d_\phi}$, where C is some constant and $d_\phi = d_r - 1$. Note that since $\phi^2(t)$ enters the definition of $r_{\text{eff}}(t)$, cf. Eq. (9), the more dominant scaling t^{-d_r+1} from the OP must be compensated by the trans-

verse correlations. On the other hand, from the previous paragraph, we deduce $\delta n_{\text{tot}}^\perp \sim t^{\alpha-\beta}$, and, therefore:

$$\alpha - \beta = -d_r + 1 \Rightarrow d_r = 1 + \beta - \alpha = \frac{5}{2}. \quad (17)$$

This result also gives $d_\phi = d_r - 1 = \frac{3}{2}$. The above analysis has explained all long-time scalings. Note, however, that the self-similarity in Eq. (14) settles much earlier than the final relaxation stage. It is striking that the functional form of $f(x)$, cf. Eq. (14), is the same for the last two dynamical stages (Fig. 4), an interesting feature that warrants further investigation.

It is worth mentioning that there are two well-known scenarios – (i) critical ageing dynamics^{57–60} and (ii) phase ordering kinetics^{45,46,56} – where self-similar dynamics is well established in an overdamped $O(N)$ model. Scenario (i) focuses on a temperature quench specifically to a critical point, which is not applicable here. By contrast, scenario (ii) shares some similarities with the above physical picture. The usual phase ordering kinetics is concerned with a quench from the disordered phase to a temperature below T_c , which parallels our quenching protocol, where the OP becomes initially suppressed and then slowly recovers to its equilibrium value. Another resemblance is that the two scenarios share the same exponent $\beta = \frac{1}{2}$. However, in the phase ordering kinetics, the classical field expectation value cannot develop, as trivially follows from Eq. (6), and the origin of the self-similarity is due to the growth of large phase-coherent competing domains. By contrast, the self-similarity in our case is due to the interplay between the nonzero OP ϕ and proliferating fluctuations, resulting in new exponents $d_\phi = \frac{3}{2}$ and $d_r = \frac{5}{2}$. The initial conditions also seem to be very different: In the phase-ordering case, one often starts from high temperatures with profound thermal fluctuations, cf. Eq. (10); here, at the time when the OP becomes suppressed, fluctuations become depleted instead of proliferated.

V. DISCUSSION AND OUTLOOK

This section is devoted to addressing the applicability of our results to real experiments. In Section I, we motivated our study with recurring phenomenology observed in a wide variety of materials. We believe that our framework describes the underlying physics of these systems qualitatively; however, due to several features specific to each of these materials, it may alter the quantitative description. Here are some sources for potential quantitative disagreement. First, our theory is based on (3+1)-dimension, but most of those materials are either quasi-one-dimensional, such as $\text{K}_{0.3}\text{MoO}_3$ ^{17,26}, or quasi-two-dimensional, including rare-earth tritellurides^{18–22}, TiSe_2 ²³, and cuprates¹⁵. Second, in multiple cases, such as Ni_2MnGa ³², several distinct, potentially competing orders are essential. Third, systems with additional (often approximate) symmetries, such as magnetic

Sr_2IrO_4 ³¹, are beyond the non-conserved OP evolution studied here. Fourth, some experiments reported coherent Higgs-like oscillations^{17,19,26,32}, which are neglected in the overdamped dynamics considered here. The latter also implies that the model-A formalism disregards the so-called short-time dynamical slowing-down²¹. Given these complications, it seems quite striking that these materials demonstrate similar behavior in pump-probe experiments.

Our work suggests that behind this common phenomenology is a simple, intuitive interpretation where slow overpopulated Goldstone modes dominate the system evolution after photoexcitation. We make a few observations to address the complications noted in the previous paragraph. First, in quasi-1D or 2D systems, fluctuations are expected to be more significant compared to 3D. Hence, we anticipate a similar, if not more pronounced proliferation of Goldstone modes. Second, one can straightforwardly extend the present framework to account for several orders^{61,62}, and it would be intriguing to see how enhanced fluctuations enter the interplay between different orders. Third, in magnetic systems⁹ with additional approximate symmetries, our results suggest that rapidly-growing, nonthermal magnons will dominate the system dynamics. We leave the conserved OP dynamics for future work. Fourth, coherent dynamics^{63,64}, such as Higgs-like oscillations, is not expected to dictate the evolution for a strong pulse because these oscillations are expected to be overdamped. From a practical point of view, the model-A dynamics should also be a good approximation to describe experiments that have an in-

sufficient time resolution to detect oscillatory behavior. On experimental side, it is essential to verify our interpretation.

Finally, we note that a variety of time-resolved experiments could be performed to test our predictions. Examples include electron or x-ray diffuse scattering⁶⁵⁻⁶⁷, resonant inelastic x-ray scattering¹⁵, and Brillouin scattering⁶⁸. These experiments give access to momentum- and/or energy-resolved dynamics of bosonic excitations related to OP, so one may specifically search for signatures of: (i) non-thermal population of the transverse modes, (ii) the self-similarity encoded in Eq. (14), and (iii) different dynamical stages after photoexcitation (Fig. 1c).

ACKNOWLEDGMENTS

The authors would like to thank A. Kogar, B.V. Fine, A.E. Tarkhov, A. Bedrova, V. Kasper, S.L. Johnson, J. Rodriguez-Nieva, J. Marino, A. Schuckert, A. Cavalleri, G. Falkovich, and Z.-X. Shen for fruitful discussions. N.G. and A.Z. acknowledge support from the U.S. Department of Energy, BES DMSE and the Skoltech NGP Program (Skoltech-MIT joint project). P.E.D., M.H.M., and E.D. were supported by the Harvard-MIT Center of Ultracold Atoms, AFOSR-MURI Photonic Quantum Matter (award FA95501610323), and DARPA DRINQS program (award D18AC00014).

* Correspondence to: p.dolgirev@g.harvard.edu

¹ N. Goldenfeld, *Lectures on Phase Transitions and the Renormalization Group* (Addison-Wesley, 1992).

² K. Schwarz, *Phys. Rev. B* **38**, 2398 (1988).

³ R. Micha and I. I. Tkachev, *Phys. Rev. Lett.* **90**, 121301 (2003).

⁴ R. Micha and I. I. Tkachev, *Phys. Rev. D* **70**, 043538 (2004).

⁵ J. Berges, A. Rothkopf, and J. Schmidt, *Phys. Rev. Lett.* **101**, 041603 (2008).

⁶ J. Berges and D. Sexty, *Phys. Rev. D* **83**, 085004 (2011).

⁷ B. Nowak, J. Schole, D. Sexty, and T. Gasenzer, *Phys. Rev. A* **85**, 043627 (2012).

⁸ A. P. Orioli, K. Boguslavski, and J. Berges, *Phys. Rev. D* **92**, 025041 (2015).

⁹ S. Bhattacharyya, J. F. Rodriguez-Nieva, and E. Demler, arXiv:1908.00554 (2019).

¹⁰ B. Nowak, D. Sexty, and T. Gasenzer, *Phys. Rev. B* **84**, 020506 (2011).

¹¹ S. Erne, R. Bücker, T. Gasenzer, J. Berges, and J. Schmiedmayer, *Nature* **563**, 225 (2018).

¹² M. Prüfer, P. Kunkel, H. Strobels, S. Lannig, D. Linne-mann, C.-M. Schmied, J. Berges, T. Gasenzer, and M. K. Oberthaler, *Nature* **563**, 217 (2018).

¹³ C. Eigen, J. A. Glidden, R. Lopes, E. A. Cornell, R. P. Smith, and Z. Hadzibabic, *Nature* **563**, 221 (2018).

¹⁴ N. Navon, A. L. Gaunt, R. P. Smith, and Z. Hadzibabic, *Nature* **539**, 72 (2016).

¹⁵ M. Mitrano, S. Lee, A. A. Husain, L. Delacretaz, M. Zhu, G. de la Peña Muñoz, S. X.-L. Sun, Y. I. Joe, A. H. Reid, S. F. Wandel, *et al.*, *Sci. Adv.* **5**, eaax3346 (2019).

¹⁶ G. I. Barenblatt and B. G. Isaakovich, *Scaling, self-similarity, and intermediate asymptotics: dimensional analysis and intermediate asymptotics*, Vol. 14 (Cambridge University Press, 1996).

¹⁷ A. Tomeljak, H. Schaefer, D. Städter, M. Beyer, K. Biljakovic, and J. Demsar, *Phys. Rev. Lett.* **102**, 066404 (2009).

¹⁸ F. Schmitt, P. S. Kirchmann, U. Bovensiepen, R. Moore, J. Chu, D. Lu, L. Rettig, M. Wolf, I. Fisher, and Z. Shen, *New J. Phys.* **13**, 063022 (2011).

¹⁹ A. Zong, A. Kogar, Y.-Q. Bie, T. Rohwer, C. Lee, E. Baldini, E. Ergeçen, M. B. Yilmaz, B. Freelon, E. J. Sie, *et al.*, *Nat. Phys.* **15**, 27 (2019).

²⁰ A. Kogar, A. Zong, P. E. Dolgirev, X. Shen, J. Straquadine, Y.-Q. Bie, X. Wang, T. Rohwer, I. Tung, Y. Yang, *et al.*, *Nat. Phys.* **16**, 159 (2020).

²¹ A. Zong, P. E. Dolgirev, A. Kogar, E. Ergeçen, M. B. Yilmaz, Y.-Q. Bie, T. Rohwer, I.-C. Tung, J. Straquadine, X. Wang, *et al.*, *Phys. Rev. Lett.* **123**, 097601 (2019).

²² F. Zhou, J. Williams, C. D. Malliakas, M. G. Kanatzidis, A. F. Kemper, and C.-Y. Ruan, arXiv eprint:1904.07120

- (2019).
- ²³ E. Möhr-Vorobeva, S. L. Johnson, P. Beaud, U. Staub, R. De Souza, C. Milne, G. Ingold, J. Demsar, H. Schaefer, and A. Titov, *Phys. Rev. Lett.* **107**, 036403 (2011).
- ²⁴ C. Laulhé, T. Huber, G. Lantz, A. Ferrer, S. O. Mariager, S. Grübel, J. Rittmann, J. A. Johnson, V. Esposito, A. Lübcke, *et al.*, *Phys. Rev. Lett.* **118**, 247401 (2017).
- ²⁵ S. Vogelgesang, G. Storeck, J. Horstmann, T. Diekmann, M. Sivis, S. Schramm, K. Rosnagel, S. Schäfer, and C. Ropers, *Nat. Phys.* **14**, 184 (2018).
- ²⁶ T. Huber, S. O. Mariager, A. Ferrer, H. Schäfer, J. A. Johnson, S. Grübel, A. Lübcke, L. Huber, T. Kubacka, C. Dornes, *et al.*, *Phys. Rev. Lett.* **113**, 026401 (2014).
- ²⁷ G. Storeck, J. G. Horstmann, T. Diekmann, S. Vogelgesang, G. von Witte, S. Yalunin, K. Rosnagel, and C. Ropers, arXiv:1909.10793 (2019).
- ²⁸ S. Hellmann, T. Rohwer, M. Källäne, K. Hanff, C. Sohrt, A. Stange, A. Carr, M. Murnane, H. Kapteyn, L. Kipp, *et al.*, *Nat. Commun.* **3**, 1069 (2012).
- ²⁹ K. Okazaki, Y. Ogawa, T. Suzuki, T. Yamamoto, T. Someya, S. Michimae, M. Watanabe, Y. Lu, M. No-hara, H. Takagi, *et al.*, *Nat. Commun.* **9**, 4322 (2018).
- ³⁰ A. Kirilyuk, A. V. Kimel, and T. Rasing, *Rev. Mod. Phys.* **82**, 2731 (2010).
- ³¹ M. Dean, Y. Cao, X. Liu, S. Wall, D. Zhu, R. Mankowsky, V. Thampy, X. Chen, J. Vale, D. Casa, *et al.*, *Nat. Mater.* **15**, 601 (2016).
- ³² S. Mariager, C. Dornes, J. Johnson, A. Ferrer, S. Grübel, T. Huber, A. Caviezel, S. Johnson, T. Eichhorn, G. Jakob, *et al.*, *Phys. Rev. B* **90**, 161103 (2014).
- ³³ P. Beaud, A. Caviezel, S. O. Mariager, L. Rettig, G. Ingold, C. Dornes, S.-W. Huang, J. A. Johnson, M. Radovic, T. Huber, *et al.*, *Nat. Mater.* **13**, 923 (2014).
- ³⁴ Z. Tao, T.-R. T. Han, and C.-Y. Ruan, *Phys. Rev. B* **87**, 235124 (2013).
- ³⁵ B. Mansart, D. Boschetto, A. Savoia, F. Rullier-Albenque, F. Bouquet, E. Papalazarou, A. Forget, D. Colson, A. Rousse, and M. Marsi, *Phys. Rev. B* **82**, 024513 (2010).
- ³⁶ L. Perfetti, P. Loukakos, M. Lisowski, U. Bovensiepen, H. Eisaki, and M. Wolf, *Phys. Rev. Lett.* **99**, 197001 (2007).
- ³⁷ P. E. Dolgirev, A. Rozhkov, A. Zong, A. Kogar, N. Gedik, and B. V. Fine, arXiv eprint:1904.09795 (2019).
- ³⁸ S. L. Johnson, M. Savoini, P. Beaud, G. Ingold, U. Staub, F. Carbone, L. Castiglioni, M. Hengsberger, and J. Osterwalder, *Struct. Dyn.* **4**, 061506 (2017).
- ³⁹ Since OP degrees of freedom are composed of electrons and phonons, the introduction of three subsystems might be confusing. For this reason, in CDW systems one sometimes splits the lattice into two groups: (i) phonons associated with the OP and (ii) the rest of the lattice. One then describes a non-equilibrium state by assigning different temperatures to each subsystem.
- ⁴⁰ N. Gedik, P. Blake, R. Spitzer, J. Orenstein, R. Liang, D. Bonn, and W. Hardy, *Phys. Rev. B* **70**, 014504 (2004).
- ⁴¹ P. Kusar, V. V. Kabanov, J. Demsar, T. Mertelj, S. Sugai, and D. Mihailovic, *Phys. Rev. Lett.* **101**, 227001 (2008).
- ⁴² R. P. Prasankumar and A. J. Taylor, *Optical techniques for solid-state materials characterization* (CRC Press, 2016).
- ⁴³ F. Boschini, E. da Silva Neto, E. Razzoli, M. Zonno, S. Peli, R. Day, M. Michiardi, M. Schneider, B. Zwartsenberg, P. Nigge, *et al.*, *Nat. Mater.* **17**, 416 (2018).
- ⁴⁴ P. C. Hohenberg and B. I. Halperin, *Rev. Mod. Phys.* **49**, 435 (1977).
- ⁴⁵ G. F. Mazenko and M. Zannetti, *Phys. Rev. B* **32**, 4565 (1985).
- ⁴⁶ M. Zannetti, *J. Phys. A* **26**, 3037 (1993).
- ⁴⁷ A. Chandran, A. Nanduri, S. S. Gubser, and S. L. Sondhi, *Phys. Rev. B* **88**, 024306 (2013).
- ⁴⁸ B. Sciolla and G. Biroli, *Phys. Rev. B* **88**, 201110 (2013).
- ⁴⁹ A. Chiochetta, M. Tavora, A. Gambassi, and A. Mitra, *Phys. Rev. B* **91**, 220302 (2015).
- ⁵⁰ A. Maraga, A. Chiochetta, A. Mitra, and A. Gambassi, *Phys. Rev. E* **92**, 042151 (2015).
- ⁵¹ A. Chiochetta, M. Tavora, A. Gambassi, and A. Mitra, *Phys. Rev. B* **94**, 134311 (2016).
- ⁵² J. Berges, in *AIP Conf. Proc.*, Vol. 739 (American Institute of Physics, 2004) pp. 3–62.
- ⁵³ V. E. Zakharov, V. S. L'vov, and G. Falkovich, *Kolmogorov spectra of turbulence I: Wave turbulence* (Springer Science & Business Media, 2012).
- ⁵⁴ S. Nazarenko, *Wave turbulence*, Vol. 825 (Springer Science & Business Media, 2011).
- ⁵⁵ M. Mondello and N. Goldenfeld, *Physical Review A* **45**, 657 (1992).
- ⁵⁶ A. J. Bray, *Adv. Phys.* **51**, 481 (2002).
- ⁵⁷ H. Janssen, B. Schaub, and B. Schmittmann, *Z. Phys. B* **73**, 539 (1989).
- ⁵⁸ P. Calabrese and A. Gambassi, *J. Phys. A* **38**, R133 (2005).
- ⁵⁹ M. Henkel and M. Pleimling, *Non-Equilibrium Phase Transitions: Volume 2: Ageing and Dynamical Scaling Far from Equilibrium* (Springer Science & Business Media, 2011).
- ⁶⁰ U. C. Täuber, *Critical dynamics: a field theory approach to equilibrium and non-equilibrium scaling behavior* (Cambridge University Press, 2014).
- ⁶¹ Z. Sun and A. J. Millis, arXiv eprint: 1905.05341 (2019).
- ⁶² H. Schaefer, V. V. Kabanov, and J. Demsar, *Phys. Rev. B* **89**, 045106 (2014).
- ⁶³ P. Gagel, P. P. Orth, and J. Schmalian, *Phys. Rev. Lett.* **113**, 220401 (2014).
- ⁶⁴ P. Gagel, P. P. Orth, and J. Schmalian, *Phys. Rev. B* **92**, 115121 (2015).
- ⁶⁵ T. Chase, M. Trigo, A. H. Reid, R. Li, T. Vecchione, X. Shen, S. Weathersby, R. Coffee, N. Hartmann, D. A. Reis, X. J. Wang, and H. A. Dürr, *Appl. Phys. Lett.* **108**, 041909 (2016).
- ⁶⁶ S. Wall, S. Yang, L. Vidas, M. Chollet, J. M. Glownia, M. Kozina, T. Katayama, T. Henighan, M. Jiang, T. A. Miller, *et al.*, *Science* **362**, 572 (2018).
- ⁶⁷ M. J. Stern, L. P. René de Cotret, M. R. Otto, R. P. Chate-lain, J.-P. Boisvert, M. Sutton, and B. J. Siwick, *Phys. Rev. B* **97**, 165416 (2018).
- ⁶⁸ S. O. Demokritov, B. Hillebrands, and A. N. Slavin, *Phys. Rep.* **348**, 441 (2001).

Appendix A: Derivation of the equations of motion

Here we provide details of the derivation of the main Eqs. (6)–(9).

Dynamics of ϕ . Evolution of the field $\phi = \frac{1}{\sqrt{V}}\phi_{1,\mathbf{q}=0}$ can be obtained from:

$$\partial_t \langle \phi_{\alpha,\mathbf{q}} \rangle_t = \int D[\phi] \phi_{\alpha,\mathbf{q}} \partial_t \mathcal{P}([\phi], t) = -\Gamma \left\langle \frac{\delta \mathcal{F}}{\delta \phi_{\alpha,-\mathbf{q}}} \right\rangle, \quad (\text{A1})$$

where in the last equality we used the Fokker-Planck Eq. (5), and integration by parts. The latter derivative can be calculated from Eq. (3):

$$\frac{\delta \mathcal{F}}{\delta \phi_{\alpha, -\mathbf{q}}} = (r + K\mathbf{q}^2)\phi_{\alpha, \mathbf{q}} + \frac{4u}{V} \sum_{\mathbf{k}_1, \mathbf{k}_2} \phi_{\beta, \mathbf{k}_1} \phi_{\beta, \mathbf{k}_2} \phi_{\alpha, \mathbf{q} - \mathbf{k}_1 - \mathbf{k}_2}. \quad (\text{A2})$$

Using Wick's theorem and leaving only terms up to the leading order in $1/N$, we obtain

$$\left\langle \sum_{\mathbf{k}_1, \mathbf{k}_2} \phi_{\beta, \mathbf{k}_1} \phi_{\beta, \mathbf{k}_2} \phi_{1, -\mathbf{k}_1 - \mathbf{k}_2} \right\rangle \approx \phi_{1, \mathbf{q}=0}^3 + \phi_{1, \mathbf{q}=0} \sum_{\mathbf{k}} (D_{\mathbf{k}}^{\parallel} + (N-1)D_{\mathbf{k}}^{\perp}). \quad (\text{A3})$$

Combining Eq. (A1) and Eq. (A3) we arrive at Eq. (6) of the main text.

Dynamics of the correlators. Applying the same trick as above, we derive:

$$\begin{aligned} \partial_t \langle \phi_{\alpha, \mathbf{k}} \phi_{\alpha, -\mathbf{k}} \rangle_c &= 2T\Gamma - 2\Gamma \times \\ &\times \left[\left\langle \phi_{\alpha, \mathbf{k}} \frac{\delta F}{\delta \phi_{\alpha, \mathbf{k}}} \right\rangle - \langle \phi_{\alpha, \mathbf{k}} \right\rangle \left\langle \frac{\delta F}{\delta \phi_{\alpha, \mathbf{k}}} \right\rangle \right]. \end{aligned} \quad (\text{A4})$$

For the case of the transverse component, in the leading in $1/N$ order we obtain:

$$\begin{aligned} \left\langle \phi_{\alpha, \mathbf{k}} \sum_{\mathbf{k}_1, \mathbf{k}_2} \phi_{\beta, \mathbf{k}_1} \phi_{\beta, \mathbf{k}_2} \phi_{\alpha, -\mathbf{k} - \mathbf{k}_1 - \mathbf{k}_2} \right\rangle &\approx \\ \approx D_{\mathbf{k}}^{\perp} \left(\phi_{1, \mathbf{q}=0}^2 + \sum_{\mathbf{q}} (D_{\mathbf{q}}^{\parallel} + (N-1)D_{\mathbf{q}}^{\perp}) \right). \end{aligned} \quad (\text{A5})$$

Combining Eq. (A4) and Eq. (A5) we arrive at Eq. (7) of the main text. For the case of the longitudinal component, similarly to the above discussion we get

$$\begin{aligned} \sum_{\mathbf{k}_1, \mathbf{k}_2} \left(\langle \phi_{1, \mathbf{k}} \phi_{\beta, \mathbf{k}_1} \phi_{\beta, \mathbf{k}_2} \phi_{1, -\mathbf{k} - \mathbf{k}_1 - \mathbf{k}_2} \rangle - \langle \phi_{1, \mathbf{k}} \rangle \langle \phi_{\beta, \mathbf{k}_1} \phi_{\beta, \mathbf{k}_2} \phi_{1, -\mathbf{k} - \mathbf{k}_1 - \mathbf{k}_2} \rangle \right) &\approx \\ \approx D_{\mathbf{k}}^{\parallel} \left(3\phi_{1, \mathbf{q}=0}^2 + \sum_{\mathbf{q}} (D_{\mathbf{q}}^{\parallel} + (N-1)D_{\mathbf{q}}^{\perp}) \right). \end{aligned} \quad (\text{A6})$$

This equation leads to Eq. (8).

Appendix B: Longitudinal correlations at long times

During the evolution, the longitudinal correlation function $D_{\mathbf{k}}^{\parallel}$ remains bell-shaped with a maximum at $k = 0$ suggesting to define $\tilde{g}(t) = D_{k=0}^{\parallel}(t)$ and $k_{\parallel}^*(t)$ to be the wave vector corresponding to half width at half maximum in $D_{\mathbf{k}}^{\parallel}$. Notably, both functions at long times behave as $\tilde{g}(t), k_{\parallel}^*(t) \sim t^{-d_{\phi}}$ – see Fig. 5. We also observe that this

power-law exponent implies that the longitudinal correlations exhibit the leading scaling, i.e. these modes should not be entirely ignored.

To explain the above observation, we note that at long times, when the order parameter $\phi(t) = \phi_0 + \delta\phi$ is already close to be recovered, the equation of motion (8) can be approximated to (we fix $K = 1$ for convenience)

$$\frac{d\delta D_{\mathbf{k}}^{\parallel}}{dt} \approx -32\Gamma u \phi_0 \delta\phi D_{\mathbf{k}, \text{eq}}^{\parallel} - 2\Gamma(k^2 + 8u\phi_0^2)\delta D_{\mathbf{k}}^{\parallel}, \quad (\text{B1})$$

where $D_{\mathbf{k}}^{\parallel}(t) = D_{\mathbf{k}, \text{eq}}^{\parallel} + \delta D_{\mathbf{k}}^{\parallel}(t)$ and we disregarded fast $r_{\text{eff}}(t) \sim t^{-d_r}$ compared to slow $\delta\phi(t) \sim t^{-d_{\phi}}$ ($0 < d_{\phi} < d_r$). The above equation can be solved analytically. Indeed, substituting $\delta D_{\mathbf{k}}^{\parallel}(t) = e^{-2\Gamma(k^2 + 8u\phi_0^2)t} h_{\mathbf{k}}(t)$, we obtain the following equation on $h_{\mathbf{k}}(t)$:

$$\frac{dh_{\mathbf{k}}}{dt} = -32\Gamma u \phi_0 \delta\phi D_{\mathbf{k}, \text{eq}}^{\parallel} e^{2\Gamma(k^2 + 8u\phi_0^2)t}. \quad (\text{B2})$$

Integration of this equation gives

$$h_{\mathbf{k}}(t) = h_{\mathbf{k}}(t_0) + \frac{C}{k^2 + 8u\phi_0^2} \int_{t_0}^t dt' \frac{e^{2\Gamma(k^2 + 8u\phi_0^2)t'}}{(t')^{d_{\phi}}}, \quad (\text{B3})$$

where C is some constant. We, therefore, conclude that

$$\delta D_{\mathbf{k}}^{\parallel} = \delta D_{\mathbf{k}}^{\parallel, (1)} + \delta D_{\mathbf{k}}^{\parallel, (2)}, \quad (\text{B4})$$

where $\delta D_{\mathbf{k}}^{\parallel, (1)}(t) = h_{\mathbf{k}}(t_0) e^{-2\Gamma(k^2 + 8u\phi_0^2)t}$ decays exponentially in time, whereas

$$\delta D_{\mathbf{k}}^{\parallel, (2)} \sim \frac{e^{-2\Gamma(k^2 + 8u\phi_0^2)t}}{k^2 + 8u\phi_0^2} \int_{t_0}^t dt' \frac{e^{2\Gamma(k^2 + 8u\phi_0^2)t'}}{(t')^{d_{\phi}}} \quad (\text{B5})$$

is potentially important.

At long times $t \rightarrow \infty$, we observe that

$$F(t) \equiv \int_{t_0}^t dt' \frac{e^{at'}}{(t')^b} \sim \frac{e^{at}}{t^b}, \quad a, b > 0. \quad (\text{B6})$$

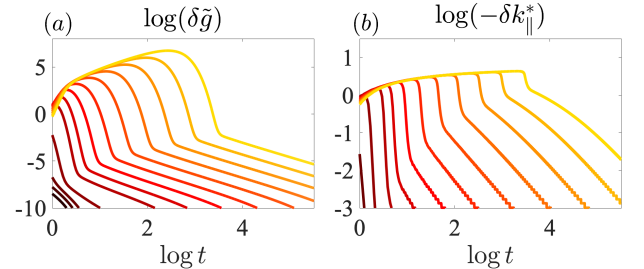


FIG. 5. (a) evolution of the scaling function $\delta\tilde{g}(t) \equiv \tilde{g}(t) - \tilde{g}_{\text{eq}}$ for different quenches. (b) the same for the longitudinal wave vector $\delta k_{\parallel}^*(t) \equiv k_{\parallel}^*(t) - k_{\parallel, \text{eq}}^*$. The second (inflation) and the third (mode decoupling) stages of the overall dynamics are clearly seen. At long times, both functions scale as $\delta\tilde{g}(t), \delta k_{\parallel}^*(t) \sim t^{-d_{\phi}}$.

Indeed, by differentiating $F(t)$ we note that it satisfies

$$\frac{dF}{dt} = \frac{e^{at}}{t^b}. \quad (\text{B7})$$

By substituting $F(t) = e^{at}p(t)$ we separate rapid exponential growth from slow power-law-like dynamics encoded in $p(t)$:

$$\frac{dp}{dt} + ap = \frac{1}{t^b}. \quad (\text{B8})$$

From this equation, we finally see that $p \sim t^{-b}$ (as long

as $a \neq 0$). Combining Eqs. (B5) and (B6), we conclude that

$$\delta D_{\mathbf{k}}^{\parallel,(2)} \sim \frac{t^{-d_\phi}}{k^2 + 8u\phi_0^2}, \quad (\text{B9})$$

i.e. indeed $\delta D_{\mathbf{k}}^{\parallel}$ gets power-law-like contribution with the leading exponent. For completeness, we also note that

$$\delta n_{\text{tot}}^{\parallel,(2)} = \int \frac{d^3\mathbf{k}}{(2\pi)^3} \delta D_{\mathbf{k}}^{\parallel,(2)} \sim t^{-d_\phi} \quad (\text{B10})$$

also exhibits the same scaling.